150-mJ 1550-nm KTA OPO with good beam quality and high efficiency

Darrell J. Armstrong and Arlee V. Smith

Dept. 1118, Sandia National Laboratories, Albuquerque, NM 87185-1423, USA

ABSTRACT

We've demonstrated a nanosecond KTA OPO utilizing a high Fresnel-number quasi-monolithic image-rotating nonplanar-ring optical cavity to efficiently generate 1550 nm light with beam quality $M^2 \sim 4$. The OPO was pumped at 1064 nm and injection-seeded at 1550 nm and was tested using either one or two $10\times10\times17$ mm^3 KTA crystals. Total measured conversion efficiencies were as high as 45% and 55% respectively, with corresponding 1550 nm energies of approximately 135 mJ and 170 mJ. While energy and efficiency were high, agreement with numerical models that included walkoff, diffraction, and geometry of the nonplanar-ring, was poor near the oscillation threshold. Single-crystal oscillation revealed different thresholds for each KTA crystal. When tested by observing unphasematched 2ω generation, each crystal appears to contain a single ferroelectric domain, suggesting that refractive index inhomogeneity, or some other type of defect, prevents perfect phasematching.

Keywords: Nonlinear optics, optical parametric oscillator, image rotation, nonplanar ring oscillator

1. INTRODUCTION

There has long been a need for efficient high-energy light sources with good beam quality operating in the eyesafe spectral region near $\lambda \approx 1550$ nm. Nanosecond OPO's based on crystals such as $LiNbO_3$, KTP, or KTA pumped by the Nd:YAG fundamental at $\lambda = 1064$ nm are attractive for this application, generating signal and idler waves near 1500–1600 nm and 3200–3600 nm, respectively. However, pulse energies $\gtrsim 100$ mJ require large beam diameters to avoid optical damage, resulting in high-$\mathcal{F}$ cavities, where $\mathcal{F}$ denotes the Fresnel number.* Unfortunately, OPO's using high-$\mathcal{F}$ cavities rival flashlights for generating poor-quality beams, making them impractical for many applications. To resolve the high-$\mathcal{F}$ problem, and build a useful $\lambda = 1550$ nm OPO, we employ a robust, quasi-monolithic, image-rotating OPO cavity that allows large diameter beams but delivers excellent beam quality. The image-rotating OPO in this report uses the crystal KTA.

Early in its development, KTA was shown to efficiently generate near- to mid-IR pulses when pumped with 1064 nm light.[1] KTA has adequately large d_{eff}, higher damage thresholds than $LiNbO_3$, and IR transmission in the 3–4 μm range better than that of KTP. In addition, the x-cut of KTA noncritically phasematches in the range of communication wavelengths at $\lambda = 1534.7$ nm. While KTA possesses desirable attributes, it may not be as well developed as other crystals. Our measurements indicate lower than anticipated conversion efficiency, suggesting inhomogeneous refractive indices or other manufacturing or contamination related defects that inhibit phasematching near $\Delta k = 0$. In fact, the literature on KTA OPO's suggests others have had similar problems. There are many successful examples of near- to mid-IR generation using femtosecond pulses,[2–7] where a "good" crystal of length ~ 1 mm is easily obtained. On the other hand, there are fewer examples of nanosecond[8–11] or cw[12] operation using KTA for this spectral range, where much longer crystals are required.

In our experiments, we used either one or two $10 \times 10 \times 17$ mm^3 crystals in the OPO cavity. Although we obtained reasonably high efficiency and acceptable beam quality at $\lambda = 1550$ nm for either one- or two-crystal configurations, our measured oscillation thresholds agreed poorly with a well-tested model.[13,14] These disagreements led to thorough investigation of the OPO's operating parameters, including a preliminary evaluation of the quality of the KTA crystals. Although unresolved questions remain, we now suspect defective crystals are responsible for these discrepancies. While there may be problems with our two samples of KTA, we believe high-quality KTA would be ideal for high-energy near- to mid-IR applications.

Further author information: Send correspondence to D. J. Armstrong
E-mail: darmstr@sandia.gov, Telephone: 505 844 4757

*The Fresnel number, $\mathcal{F}$ is proportional to $D^2_{\text{pump}}/\lambda L_{\text{cavity}}$, and indicates the number of Fresnel zones contained in the cavity mode, where D denotes beam diameter and L the length of the cavity.

Nonlinear Frequency Generation and Conversion: Materials, Devices, and Applications III, edited by Kenneth L. Schepler, Dennis D. Lowenthal, Proceedings of SPIE Vol. 5337 (SPIE, Bellingham, WA, 2004) · 0277-786X/04/$15 · doi: 10.1117/12.528436

2. HIGH FRESNEL-NUMBER QUASI-MONOLITHIC IMAGE-ROTATING NONPLANAR-RING CAVITY KTA OPO

Our KTA OPO is based on a quasi-monolithic 90°-image-rotating nonplanar-ring oscillator known as the RISTRA, denoting Rotated Image Singly-Resonant Twisted RectAngle.[17] We selected the RISTRA because it is robust and simple, and because image rotation, when combined with birefringent walkoff, results in very high beam quality, even if the cavity's Fresnel number is large. For example, the RISTRA cavity is 110 mm in length, and our pump beam spatial profile was approximately 2nd-order super-Gaussian with $1/e^2$ diameter ~ 6 mm yielding a cavity Fresnel number $\gtrsim 200$. In a conventional two-mirror linear cavity OPO, especially where the pump is single-passed, similar parameters would yield very poor beam quality. However, the two-crystal KTA RISTRA, even with one wavefront-distorting crystal in the cavity, generates 1550 nm beams with $M^2 \sim 4$.[†]

The physical process of beam-cleanup using image rotation, along with design specifications and laboratory demonstrations of the RISTRA and other image-rotating cavities, has been reported in the literature.[15–19] Because this information is available elsewhere, our discussion of the RISTRA's properties will be brief. Among these properties, the most outstanding is insensitivity of signal beam-quality to pump beam quality. This is achieved by image rotation and birefringent walkoff working together to "cleanup" the beam by increasing phase and amplitude correlation across both transverse dimensions.[‡] Beam cleanup is maximized by selecting phasematching parameters so the pump and resonated wave (typically the signal) are orthogonally polarized and walkoff from each other within the crystal, while the pump and rejected wave (typically the idler) co-propagate within the crystal and share the same polarization. An example relevant to this work would resonate the 1550 nm signal with xz-cut KTA phasematching $1550(e) + 3393.4(o) \rightarrow 1064(o)$ at $\theta = 41.6°$. These optimum parameters largely prevent irregular fluence and phase aberrations of a poor-quality pump beam from being imposed on the resonated signal while allowing the pump "noise" to be carried away by the idler. The result is symmetric, round signal-beam spatial profiles in the near- and far-fields. For example, we've shown that a KTP RISTRA having $\mathcal{F} \gtrsim 300$ can generate 800 nm signal beams with $M^2 \sim 3$ when pumped by a large-diameter low-quality 532 nm pump beam.[17, 18]

Two different xz-cuts of KTA phasematch to resonate $\lambda = 1550$ nm with 1064 nm pumping. The one described above at $\theta = 41.6°$ phasematches for optimum beam quality but has $d_{\text{eff}} \approx 2$ pm/V, raising the oscillation threshold to an impractically high fluence. The other, at $\theta = 79.6°$ phasematches $1550(o) + 3393.4(e) \rightarrow 1064(o)$ and has $d_{\text{eff}} \approx 3$ pm/V, which reduces the oscillation threshold, but makes the signal beam quality more sensitive to pump beam quality. For practicality, we chose the latter, and because our pump beam quality was reasonably good, we still obtained a high quality signal beam.

3. PUMP BEAM QUALITY AND EXPERIMENTAL APPARATUS

Although beam quality of the RISTRA OPO is largely immune to poor pump beam quality, the optics and crystals in its cavity can still suffer damage from a low-quality high-energy beam. For this reason any OPO generating high-energy pulses, even the RISTRA, requires a high-energy pump laser with good beam quality. Unfortunately, few commercial Nd:YAG lasers produce good beams, especially those ubiquitous old workhorses manufactured ten or more years ago still lingering in our laboratory. Lasers of that era produce low- to poor-quality beams and are unsuitable for applications in nonlinear optics demanding high-quality beams. Because we used a ten year old laser in this work, we begin our discussion of the experimental apparatus by describing mandatory modifications to the pump laser.

3.1. Pump-Beam Quality

We pumped the OPO with a 10 Hz, 8–10 ns pulse-duration flashlamp-pumped Continuum Powerlite 9010 Nd:YAG laser manufactured in 1993. This laser has an oscillator and two amplifiers, and is injected-seeded for single-longitudinal-mode oscillation. Typical of commercial Nd:YAG lasers of its vintage, it employs over-filled amplifier

[†]Our method of measuring M^2 is based on analysis of the two-dimensional spatial fluence profiles, and is described in detail in Ref. 16. To measure M^2 for the KTA RISTRA, we used a Spiricon Pyrocam I pyroelectric camera, which has low spatial resolution due to the 100 μm pixel pitch. Nonetheless, we believe our M^2 values are valid, and are probably larger than would be obtained by less rigorous measurement methods.

[‡]Without image rotation, beam cleanup can occur only in the direction parallel to walkoff.

rods to extract maximum energy. While adequate for pumping dye lasers, where beam quality is less important, it's unsuitable for pumping OPO's. "Hot spots" in the characteristic round-aperture diffraction pattern damage tend to optical coatings. Propagation $\gtrsim$ 1–2 m further diminishes suitability as a pump beam, making relay-imaging mandatory.

To eliminate the hot spots we spatially filtered the beam from the oscillator using a 2 m focal length lens followed by a 600 μm diameter diamond wire die. Subsequent collimation with a 1 m focal length lens, followed by clipping of the Airy rings with an iris, left a transmitted central Airy disk containing $\lesssim$ 40 mJ/pulse. The beam profile at the plane of the iris was imaged onto the first amplifier with a $1/e^2$ diameter of $\sim$ 5 mm to propagate through the 9 mm diameter amplifier rods without aperture effects. Gain saturation converted the Airy profile to an approximate 2nd-order super-Gaussian, although a complete description requires higher order terms. This modified Gaussian was imaged onto the input coupler of the OPO with maximum pulse energy of $\gtrsim$ 430 mJ. Figure 1 shows example spatial fluence profiles at the OPO with and without spatial filtering.

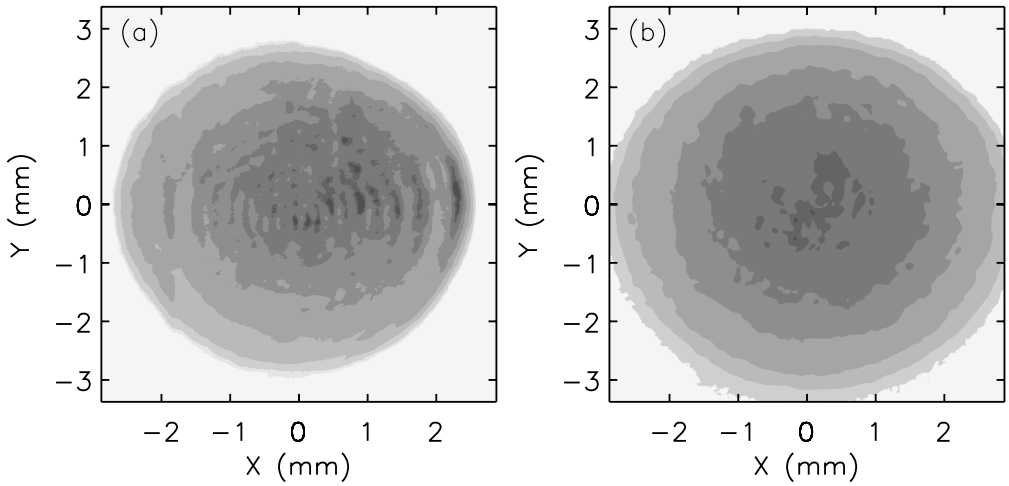

Figure 1. (a) Contour plot of typical pump-beam spatial fluence profile obtained from a commercial Nd:YAG laser with over-filled amplifier rods. The characteristic round-aperture diffraction ring pattern leads to hot spots that can damage optical coatings and crystals. (b) Contour plot of the approximate 2nd-order super-Gaussian fluence profile used to pump the OPO. The beam shown here was obtained from a modified Continuum Powerlite 9010.

While this method eliminates hot spots, the nearly-Gaussian Airy-disk inefficiently extracts energy from amplifiers and produces a less than optimum spatial profile for pumping OPO's. A better method uses beam shaping after spatial filtering to inject a near flat-top profile into the amplifiers. We plan to implement this method using a Gaussian-to-flat-top refractive shaper designed at IBM Almaden and available from Newport Corporation.[20] Improved energy extraction will better utilize laser resources and yield higher nonlinear mixing efficiency.[19]

3.2. Experimental Apparatus

A block diagram of the experiment is shown in Fig. 2. The main components are the pump laser described in Sec. 3.1, a Brewster-windowed vacuum tube for imaging the laser amplifier onto the OPO input coupler, the RISTRA OPO, a seed laser, and various diagnostics such as high-speed detectors and CCD cameras for beam profiling and alignment. Not shown are electronics and various small optical components.

The RISTRA OPO was injection seeded by a New Focus 6200 grating tuned diode laser at $\lambda = 1550$ nm, with the seed laser locked to the OPO cavity by monitoring cavity fringes. Injection seeding an OPO results in single-mode oscillation and provides useful diagnostics as well.[§] For example, collinear phasematching is simplified by

[§]Only certain OPO cavities can be injection seeded. For example, it is difficult if not impossible to injection seed a

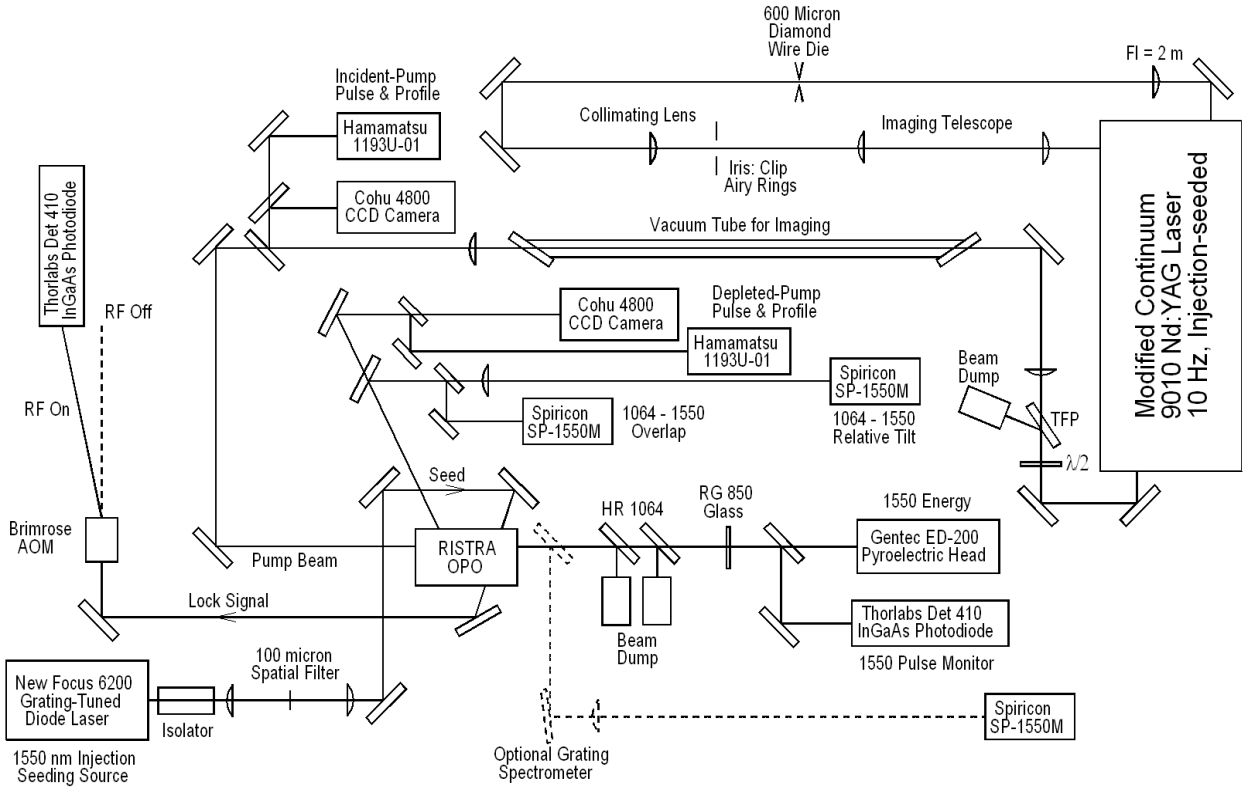

Figure 2. Block diagram of the experiment. Details of the RISTRA OPO can be found in Ref. [17]. TFP denotes thin film polarizer, AOM denotes acousto-optic modulator. See text for details.

overlapping the pump with the interferometrically aligned seed beam, and a simple grating spectrometer helps determine oscillation at $\Delta k = 0$ with respect to the seed wavelength, a useful tool for two-crystal OPO's.

The locking scheme was simple, using the reference sine-wave from a Lansing 80.215 lock-in stabilizer to modulate the diode current to generate the error signal, while the Lansing's output corrected the wavelength through the 6200's PZT input. The only difficulty was damage to the fragile InGaAs photodiode fringe detector (Thorlabs Det 410) from leakage pulses, which occurred even when the photodiode was protected by optical density > 8. An acousto-optic modulator with 270 ns risetime (Brimrose TEM-85-2) provided $\sim 100\%$ amplitude modulation to eliminate damage. With the AOM's RF drive on, the fringe-signal beam was deflected onto the detector. A few risetimes before each pulse arrived, the RF was triggered off for ~ 100 μs so the pulses missed the detector. Integrator blanking was unnecessary as the Lansing's integration time-constant is of order 1 s.

Injection seeding image-rotating cavities like the RISTRA requires lowest spatial-order seed beams because these cavities can oscillate on multi-round-trip longitudinal modes that generate optical vortices.[21] Although vortex modes are not degenerate in frequency with one-round-trip longitudinal modes, seed beams containing higher-order transverse modes complicate locking to the one-round-trip mode. Any coupling to a vortex mode diminishes beam quality and efficiency. For this reason, the astigmatic beam from the New Focus 6200 passed through a "loose" spatial filter comprised of a 150 mm lens and 100 μm pinhole before injection into the RISTRA cavity.

Spatial profiles for the incident and depleted pump were monitored by Big Sky BeamView Analyzers using Cohu 4800 CCD cameras, and incident and depleted pump-pulse powers were monitored with Hamamatsu

two-mirror linear-cavity OPO when the pump is single-passed. When the pump is double-passed, the linear cavity can be seeded.

R1193U-01 vacuum photodiodes. Spiricon SP-1550M up-conversion phosphor CCD cameras simultaneously observed cavity transmission at 1064 nm and 1550 nm in the near- and far-fields to facilitate collinear phasematching. The signal pulse energy at 1550 nm was measured using a Gentec ED-200 pyroelectric head. High-reflecting mirrors followed by RG850 absorbing glass eliminated the 1064 nm pump, 3393 nm idler, unphasematched 532 nm, and a $1064\,\text{nm} + 1550\,\text{nm} \rightarrow 630\,\text{nm}$ SFG signal, while attenuating filters reduced the 1550 nm pulse energy below the ED-200 damage threshold. Calibration was obtained by measuring transmission through these optics using the seed beam, then measuring residual 1550 nm pulse energy with a Scientech 380101 volume absorber. Pump energy was measured by placing the Scientech in front of the OPO's input coupler. Pulses from the Hamamatsu detectors and Gentec head were integrated to generate efficiency curves showing signal energy versus pump energy, and to monitor pump depletion.

4. RESULTS AND DISCUSSION

We carried out experiments to characterize the performance of the KTA RISTRA OPO, including measurements of M^2 for the 1550 nm signal beam and measurements of oscillation thresholds and conversion efficiency for comparison to predictions by numerical models. After finding discrepancies between measurements and calculations, we checked and measured many parameters affecting performance of the OPO, including an attempt to characterize the quality of the KTA crystals. Our discussion begins with the measurement of M^2.

4.1. Measurement of M^2 at $\lambda = 1550$ nm for two-crystal oscillation

We measured M^2 for two-crystal oscillation by passing the 1550 nm signal beam through a 580 mm focal length lens and recording two-dimensional spatial fluence profiles at 17 locations on both sides of the focus. Second moment waists in the directions of ordinary and extraordinary polarization were calculated and used to determine M^2. Our rigorous method is described in Ref. 16 so details are not repeated here. The only difference from our previous measurements was use of a Spiricon Pyrocam I pyroelectric camera to observe the 1550 nm light. The large 100 μm pixel size spatially integrates some higher-order structure, but the effect on measured M^2 values was minimal. A fit to measured waists in the extraordinary direction is shown in Fig. 3(a), and the 1550 nm far-field spatial fluence profile is shown in Fig. 3(b). Measurements were carried out with pump fluence 2–4 $\times$ the oscillation threshold. We measured $M^2_{\parallel} \approx 3.8$ and $M^2_{\perp} \approx 4.2$, where $\parallel$ and $\perp$ denote the directions parallel and perpendicular to birefringent walkoff.

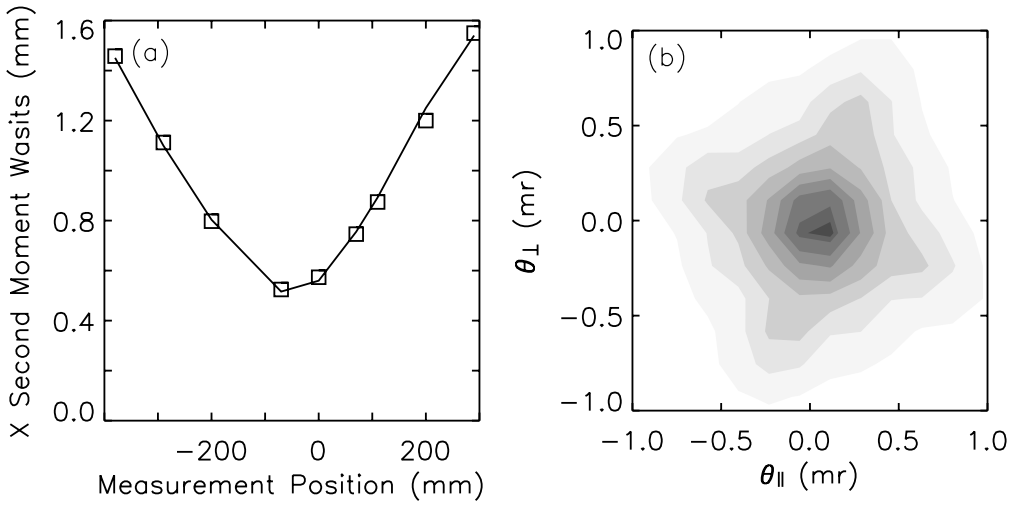

Figure 3. (a) Fit to measured second-moment waists used to determine $M^2_{\parallel}$. Data and fit for $M^2_{\perp}$ are similar. (b) Contour plot of far-field spatial fluence profile for $\lambda = 1550$ nm. The shoulder with four-fold symmetry is common to 90°-image-rotating OPO's, but the point-like structure observed here is due to a KTA crystal that distorts the beam.

All 90°-image-rotating OPO's we've studied display a weak shoulder with four-fold symmetry surrounding the central peak of the signal beam in the far-field.[16,17] The four-fold point-like structure in the shoulder in Fig. 3(b) is more pronounced than any previously observed, and is largely due to a defect in one of the crystals, as described in Sec. 4.3.

4.2. Oscillation Thresholds and Conversion Efficiencies: Comparing Measurements and Calculations

Plots of signal energy versus pump energy reliably measure oscillation thresholds and total conversion efficiencies. To verify measured efficiencies, the depleted pump was monitored as well, with percent depletion calibrated by recording transmitted pump energy when the signal circulating in the cavity was blocked. From these measurements, maximum one- and two-crystal efficiencies were as high as 45% and 55% respectively, with corresponding 1550 nm energies of approximately 135 mJ and 170 mJ.

Results for one-crystal oscillation using each crystal individually are shown in Figs. 4(a) and 4(b). Calculated efficiency curves are also displayed, with obvious discrepancies between measurements and calculations. Note the different measured oscillation thresholds and efficiency curves for the two crystals. Results for the two-

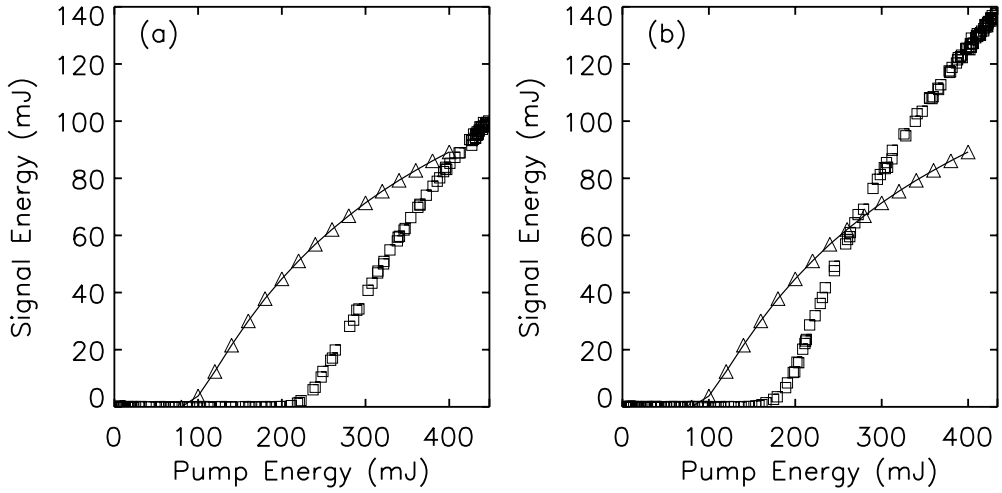

Figure 4. (a) Efficiency curve using one of two $10 \times 10 \times 17$ mm^3 KTA crystals. Boxes – measured, triangles – calculated. (b) Efficiency curve for the second of two KTA crystals. As discussed in Sec.4.3, the higher efficiency in (b) is evidently due to a focusing effect caused by an aberration in one of the crystals.

crystal RISTRA were similar, with the measured oscillation threshold approximately twice that calculated. The numerical model simulating performance of the KTA RISTRA was derived from Refs. 13 and 14, but modified for nonplanar geometry and image rotation. The unmodified model is available from Sandia Labs in the standard SNLO distribution, while various RISTRA models are available on request.[23]

Such poor agreement with a model known to accurately predict OPO performance was disappointing considering that for other OPO's we've consistently obtained agreement within a few percent.[13] To reconcile the discrepancy, parameters affecting performance including reflectance and absorbance in coatings, crystal absorbance, intracavity polarization, and transmission of the intracavity $\lambda/2$ plates, were checked and checked again, and updated in the model. The only unmeasured parameters were crystal properties such as d_{eff} or the presence of multiple ferroelectric domains, so we began to suspect disagreement was due to the crystals themselves.

4.3. Characterizing the Quality of the KTA Crystals

There are several standard tests that reveal flaws in nonlinear crystals. Some are simple, while others require more extensive measurements. We begin with a simple test to detect multiple ferroelectric domains.

4.3.1. Tests for multiple ferroelectric domains

The far-field spatial fluence profile of unphasematched 2ω generation can quickly reveal the presence of multiple ferroelectric domains, except in special cases.[24] One simply passes a fundamental beam through the crystal, focuses the 2ω light with a lens, and observes the beam pattern. We applied these tests because KTA can posses multiple domains, but found no evidence of their presence.

4.3.2. Tests of phasematching: Single-pass along the crystal's central axes

We next measured phasematching curves along the geometric central axis of each crystal. This was done by amplifying the $\lambda = 1550$ nm cw seed beam with the 1064 nm pump while monitoring the single-pass gain,

$$G = \frac{S - S_0}{S_0}, \tag{1}$$

as a function of the seed wavelength. In Eqn. 1, S is the peak power of the amplified seed and S_0 is its cw power. Baseline electronic noise, measured by simultaneously blocking the pump and cw beam, was subtracted from S and S_0. To carry out these measurements, we used the same large-diameter pump beam and sampled the gain only at the center of the crystal apertures over a small fraction of the seed-beam diameter. The powerful 1064 nm pulse was rejected by two 45° high reflectors, then completely eliminated by a 1400 nm long-pass filter. A 1 mm aperture placed in the center of the seed beam was imaged onto a low f/# lens, which focused all transmitted 1550 nm light onto 1 GHz dc-coupled detector (New Focus 1611) to compare the amplified seed to its cw power.

$\Delta k = 0$ was located by setting the wavelength-calibrated output of the New Focus 6200 to $\lambda = 1550$ nm, then angle tuning the crystals for maximum gain. Wavelengths relative to $\Delta k = 0$ were determined by counting fringes from a fused-silica solid étalon with free-spectral-range of 20.908 GHz at $\lambda = 1550$ nm. Measured and calculated curves are shown in Figs. 5(a) and 5(b), where both KTA crystals display essentially identical curves. Note that we did not compensate for dispersion in the solid étalon when plotting the data.

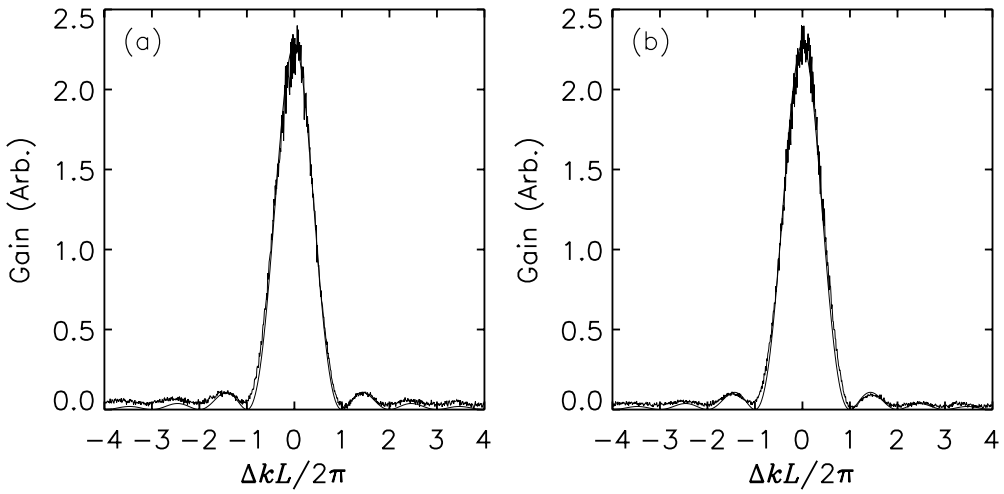

Figure 5. (a) Phasematching curve for single-pass gain at $\lambda = 1550$ nm measured along the geometric central axis of the crystal. Δk is the phase mismatch, L is the length of the crystal, and the smooth solid line is the calculated gain. As discussed in Sec.4.3.4, this crystal does not distort the transmitted wavefront. (b) Phasematching curve for crystal that severely distorts the transmitted wavefront. Evidently the aberration in the crystal does not affect phasematching along its central axis.

The results in Fig. 5 suggest near perfect phasematching, but only for rays propagating along the geometric center of each crystal. A useful complimentary measurement would be a raster-scan of gain for fixed wavelength and fixed crystal angle along many parallel paths through the crystals.

4.3.3. Tests for distortion of the transmitted wavefront

Wavefront aberrations also affect OPO performance, so we placed each crystal in a Mach-Zehnder interferometer illuminated by the large diameter 1064 nm pump beam and found one crystal distorted the transmitted wavefront. The number of waves of distortion could not be accurately determined, which suggested it was many. A subsequent single-pass measurement confirmed the distortion was severe. Contour plots for single-pass transmission of the 1064 nm beam with and without the wavefront-distorting crystal are shown in Figs. 6(a) and 6(b). The distorted profile in Fig. 6(b) is responsible for the structure in the far-field shown in Fig. 3(b). The near-field profile for single-crystal oscillation using this crystal shows a strong focusing effect, which likely explains the lower threshold and higher efficiency observed in Fig. 4(b).

We later found the aberration was easily observed with the unaided eye. Looking through the crystal revealed a wedge-shaped discontinuous change in the refractive index, extending from one side approximately halfway across the square aperture, but not traversing the center of the crystal. Nonetheless, we made no attempt to determine the exact location of the aberration within the crystal. Instead, we returned the crystal to the supplier for evaluation and replacement.[¶]

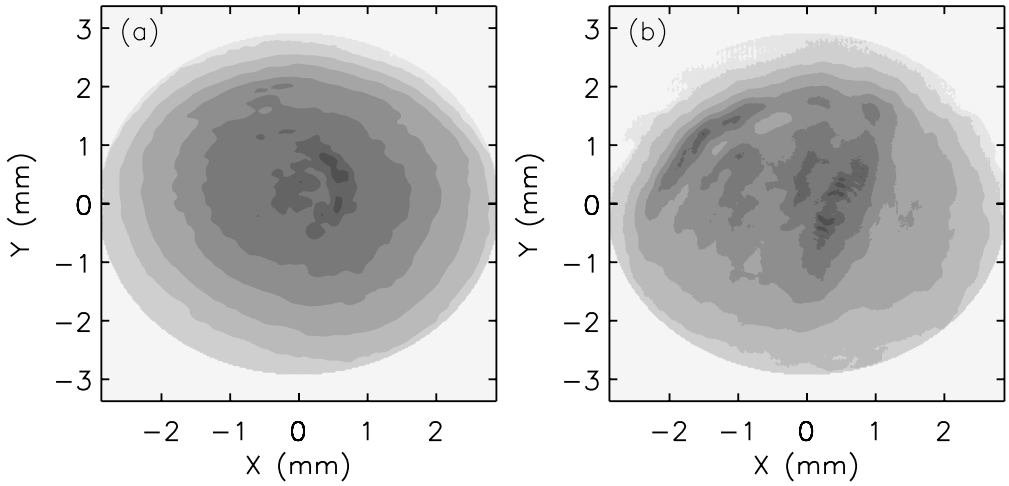

Figure 6. (a) Fluence profile for 1064 nm reference beam used to test crystals for single-pass wavefront distortion. (b) Fluence profile for 1064 nm reference beam in (a) after passing through wavefront-distorting crystal. The fluence profiles were recorded after the beams propagated ~ 1 m.

4.3.4. Measurement of d_{eff}

The wavefront-distorting crystal answered some questions, but left unresolved the high single-crystal oscillation threshold for the second crystal. While low d_{eff} could be responsible, the possibility is remote. The calculations in Sec. 4.2 suggesting higher than anticipated thresholds used $d_{\text{eff}} = 2.9$ pm/V, a reliable value for KTA obtained from earlier measurements.[25] More recent measurements of d_{eff} using KTA provided by the supplier of our $10 \times 10 \times 17$ mm^3 crystals returned a very similar value.[26] The unphasematched-2ω separated-beam method[27] used in Ref. 26 is largely immune to index inhomogeneity or other flaws, as the 2ω light is generated within one coherence length of approximately $10\,\mu$m. Because the $10 \times 10 \times 17$ mm^3 crystals require measuring d_{eff} by phasematched single-pass-gain, any flaw or inhomogeneity within the crystal would invalidate the measurement. Furthermore, simply applying low d_{eff} to a numerical model[13,14] would not accurately account for crystal anomalies that might only be described by detailed two- or three-dimensional characterization.[‖] We

[¶]The supplier of the KTA crystals, Cristal Laser, S.A., has agreed to replace the crystal that distorts the transmitted wavefront.

[‖]It should go without saying that attempting to model these anomalies, if present, would be fruitless. Efforts should be directed toward obtaining high-quality crystals.

believe the raster-scanned gain measurement described in Sec. 4.3.2 may provide more useful information than a phasematched measurement of d_{eff}.

5. CONCLUSIONS AND RECOMMENDATIONS FOR FUTURE WORK

Preliminary tests of our 1064 nm pumped 1550 nm image-rotating KTA OPO demonstrated beam quality $M^2 \sim 4$ and high efficiency. Tests were carried out using either one or two $10 \times 10 \times 17$ mm^3 crystals, with conversion efficiencies as high as 45% and 55% respectively, and corresponding 1550 nm energies of approximately 135 mJ and 170 mJ. While these results appeared promising, we found substantial discrepancies near the oscillation threshold when measurements were compared to reliable numerical models.[13,14] This was true for both one- and two-crystal oscillation. In particular, one-crystal oscillation thresholds were much higher than anticipated, and were different for each crystal.

We carefully measured all parameters affecting OPO performance, and updated our model with revised values, but the discrepancies remained. This led to thorough investigation of the KTA crystals themselves, including tests for multiple ferroelectric domains, measurements of phasematching curves, and tests for transmitted wavefront distortion. Our tests revealed no evidence of multiple domains, and we recorded nominal phasematching curves, but only for single-pass gain along the geometric center of the crystals. We subsequently recorded transmitted wavefronts, and found one crystal induced severe distortion. The aberration within that crystal was so strong it was visible to the unaided eye. That crystal has been returned to the supplier for replacement.

While wavefront distortion explained some of our observations, it did not resolve the high oscillation threshold for the remaining crystal. We doubt low d_{eff} is responsible, as recent measurements have returned similar d_{eff} values for KTA supplied by two commercial sources.[25,26] We now suspect some form of crystal inhomogeneity is responsible for the discrepancies. We plan to test for inhomogeneity by carrying out raster-scanned measurements of single-pass gain over the entire clear aperture of our remaining crystal. The results, if conclusive, will be presented in a subsequent publication.

ACKNOWLEDGMENTS

We thank Ron Allman of Sandia National Laboratories for technical assistance. We also thank Phil Hargis and Al Lang of Sandia National Laboratories for financial assistance. Sandia is a multiprogram laboratory operated by Sandia Corporation, a Lockheed Martin Company for the United States Department of Energy's National Nuclear Security Administration under contract DE-AC04-94AL85000.

REFERENCES

1. M. G. Jani, J. T. Murray, R. R. Petrin, R. C. Powell, D. N. Loiacono, and G. M. Loiacono, "Pump wavelength tuning on optical parametirc oscillations and frequency mixing in $KTiOAsO_4$," *Appl. Phys. Lett.* **60**, pp. 2327–2329, 1992.
2. P. E. Powers, S. Ramakrishna, C. L. Tang, and L. K. Cheng, "Optical parametric oscillation with $KTiOAsO_4$," *J. Opt. Soc. Am. B* **18**, pp. 1171–1173, 1993.
3. P. E. Powers, R. J. Ellingson, W. S. Pelouch, and C. L. Tang, "Recent advances of the Ti:Sapphire-pumped high-repetition-rate femtosecond optical oscillator," *J. Opt. Soc. Am. B* **10**, pp. 2162–2167, 1993.
4. D. T. Reid, C. McGowan, M. Ebrahimazadeh, and W. Sibbet, "Characterization and Modeling of a Non-collinearly Phase-Matched Femtosecond Optical Parametric Oscillator Based on KTA and Operating to Beyond 4 μm," *IEEE J. Quantum Electron.* **33**, pp. 1–9, 1997.
5. S. French, A. Miller, M. Ebrahimzadeh, "Picosecond near- to mid-infrared optical parametric oscillator using $KTiOAsO_4$," *Opt. Quantum Electron.* **29** pp. 999–1021, 1997.
6. B. Ruffing, A. Nebel, and R. Wallenstein, "All-solid-state cw mode-locked picosecond $KTiOAsO_4$ (KTA) optical parametric oscillator," *Appl. Phys. B* **67**, pp. 537–544, 1998.
7. T. Kartaloğlu and O. Aytür, "Femtosecond Self-Doubling Optical Parametric Oscillator Based on $KTiOAsO_4$", *IEEE Quantum Electron. Lett.* **39**, pp. 65–67, 2003.
8. M. S. Webb, P. F. Moulton, J. J. Kasinski, R. L. Burnham, G. Loiacono, and R. Stolzenberger, "High-averare-power $KTiOAsO_4$ optical parametric oscillator," *Opt. Lett.* **23**, pp. 1161–1163, 1998.

9. J. E. Nettleton, B. W. Schilling, D. N. Barr, and J. S. Lei, "Monoblock laser for a low-cost, eyesafe, microlaer range finder," *Appl. Opt.* **39**, pp. 2428–2432, 2000.
10. R. F. Wu, K. S. Lai, H. F. Wong, W. J. Xie, Y. L. Lim, and E. Lau, "Multiwatt mid-IR output from a Nd:YALO laser pumped intracavity KTA OPO," *Opt. Express* **8**, pp. 694–698, 2001.
11. J. M. Fukumoto "Efficient angle tunable output from a monolithic serial KTA optical parametric oscillator," OSA *Trends in Optics and Photonics* **50**, *Advanced Solid-State Lasers* pp. 675–678, 2001.
12. T. J. Edwards, G. A. Turnbull, M. H. Dunn, M. Ebrahimzadeh, and F. G. Colville, "High-power, continuous-wave, singly-resonant, intracavity optical paramtetric oscillator," *Appl. Phys. Lett.* **72**, pp. 1527–1529, 1998.
13. A. V. Smith, W. J. Alford, T. D. Raymond, and Mark S. Bowers, "Comparison of a numerical model with measured performance of nanosecond KTP optical parametric oscillator," *J. Opt. Soc. Am. B* **12**, pp. 2253–2267, 1995.
14. A. V. Smith and M. S. Bowers, "Phase distortions in sum- and difference mixing in crystals," *J. Opt. Soc. Am. B* **12**, pp. 49–57, 1995.
15. A. V. Smith and M. S. Bowers, "Image-rotating cavity designs for improved beam quality in nanosecond optical parametric oscillators," *J. Opt. Soc. Am. B* **18**, pp. 706–713, 2001.
16. D. J. Armstrong and A. V. Smith, "Demonstration of improved beam quality in an image-rotating optical parametric oscillator," *Opt. Lett.* **27**, pp. 40–42, 2002.
17. A. V. Smith and D. J. Armstrong, "Nanosecond optical parametric oscillator with 90° image rotation: Design and performance," *J. Opt. Soc. Am. B* **19**, pp. 1801–1814, 2002.
18. D. J. Armstrong and A. V. Smith, "Design and laboratory characterization of a highly efficient all solid state 200 mJ UV light source for ozone dial measurements," in *Lidar Remote Sensing for Environment Monitroing III*, U. Singh, T. Itabe, and Z. Liu, eds., *Proc. SPIE* **4893**, pp. 105–120, 2002.
19. D. J. Armstrong and A. V. Smith, "Efficient all solid-state UV source for satellite-based lidar applications," in *Lidar Remote Sensing for Environment Monitroing IV*, U. Singh, ed. *Proc. SPIE* **5154**, 2003.
20. J. A. Hoffnagle and C. M. Jefferson, "Design and performance of a refractive opticl system that converts a Gaussian to a flattop beam," *Appl. Opt.* **39**, pp. 5488–5499, 2000.
21. A. V. Smith and D. J. Armstrong, "Generation of vortex beams by an image-rotating optical parametric oscillator," *Opt. Express* **11**, pp. 868-873, 2003.
22. T. F. Johnston, "Beam propagation (M^2) measurement as easy as it gets: the four-cuts method," *Appl. Opt.* **37**. pp. 4840–4850, 1998.
23. Numerical models for the RISTRA OPO are derived from the SNLO software package, which is written and distributed by Dr. Arlee V. Smith of Sandia National Labs. SNLO contains 17 different software tools that can be used for design and testing of OPA's, OPO's, and to calculate nonlinear crystal mixing parameters. SNLO can be downloaded free of charge from http://www.sandia.gov/imrl/XWEB1128/xxtal.htm. Special codes for various versions of the one- and two-crystal image-rotating RISTRA OPO, including those for intra-cavity SFG and DFG, are available on request.
24. R. J. Gehr, W. J. Alford, and A. V. Smith, "Simple method of detecting ferroelectric domains with non-phase-matched second-harmonic generation," *Appl. Opt.* **37**, pp. 3311–3317, 1998.
25. W. J. Alford and A. V. Smith, "Wavelength variation of the second-order nonlinear coefficients of $KNbO_3$, $KTiOPO_4$, $KTiOAsO_4$, $LiNbO_3$, $LiIO_3$, β-BaB_2O_4, and LiB_3O_5 crystals: a test of Miller wavelength scaling," *JOSA B* **18**, pp. 524–533, 2001.
26. M. V. Pack, D. J. Armstrong, and A. V. Smith, "Measurement of the $\chi^{(2)}$ tensors of $KTiOPO_4$, $KTiOAsO_4$, $RbTiOPO_4$, and $RbTiOAsO_4$ crystals," *submitted to Appl. Opt.*
27. R. J. Gehr and A. V. Smith, "Seperated-beam nonphase-matched second harmonic method of characterizing nonlinear optical crystals," *J. Opt. Soc. Am. B* **15**, pp. 2298–2307, 1998.